To be published, *Journal of Directed Energy*

Thermal Damage behind HEL-Irradiated Carbon Fiber–Reinforced Polymer Skin

Jorge D. Garcia, Peter Joyce,* and Cody Brownell

United States Naval Academy, Annapolis, Maryland 21402

While lasers can defeat targets such as unmanned aerial vehicles (UAVs) through material degradation and penetration, it is also possible to defeat a target without penetration due to heat re-radiated to internal components. This possibility was investigated by using a thin carbon fiber–reinforced polymer (CFRP) to represent a UAV skin, and a steel disc to represent an internal component. A FLIR® A325sc infrared camera was used to measure temperatures on the back of the CFRP and a Type K thermocouple to measure steel disc temperature. Results confirmed that even without penetration, high energy lasers (HEL) pose a serious threat to military vehicles due to high temperatures of internal components. In addition, results indicated that the presence of the internal component near the CFRP skin contributed to even greater heating of the back surface by reflecting and radiating heat back to the CFRP. The temperature measurements using the IR camera were further validated in separate tests using a CFRP with embedded fiber Bragg grating sensors. After testing, a basic numerical model was developed and compared to the experimentally determined results. The model did not match the experiments because it was a unidimensional model and it did not account for changing material properties of the CFRP.

KEYWORDS: Carbon fiber–reinforced polymer, Unmanned aerial vehicle, Fiber Bragg gratings

Nomenclature

c_p	CFRP specific heat
c_{ps}	1008 steel specific heat
FBG	fiber Bragg grating
h	convection coefficient
HEL	high energy laser
IR	infrared
k	thermal conductivity
L	CFRP thickness
q''	heat flux
r	beam radius

Received April 20, 2015; revised June 17, 2016.
*Corresponding author; email: pjoyce@usna.edu.

T_i	initial temperature
T_1	temperature of front surface node
T_m	temperature of interior nodes
T_n	temperature of back surface node
T^p	known nodal temperature at previous time step
T^{p+1}	calculated nodal temperature at next time step
T_s	surface temperature
T_∞	air temperature/surrounding temperature
Type K	common type of thermocouple for sensors; used extensively due to reliability and accuracy at temperatures up to 1260 °C
UAV	unmanned aerial vehicle
Δt	time step
Δx	distance between nodes
$\frac{\partial T}{\partial x}$	temperature gradient
$\frac{\partial T}{\partial t}$	time rate of change in temperature
ϵ	CFRP emissivity
ϵ_s	1008 steel emissivity
ρ	CFRP density
ρ_s	1008 steel density
σ	Stefan Boltzmann constant

1. Introduction and Motivation

The Department of Defense has been researching directed energy weapons for more than 40 years due to their great potential.[1] A recent example of the military development and employment of directed energy weapons is the Navy Laser Weapon System. Also known as LaWS, this fiber-based laser weapon system was used to engage and destroy in-flight unmanned aerial vehicles (UAVs) at the Naval Air Warfare Center in China Lake, California.[2] Later, in 2014, this weapon system was deployed on the USS Ponce and allowed sailors to quickly engage and destroy drones and small boat threats, all without the use of conventional ammunition.

Just as the United States has invested heavily in directed energy weapons, so have its adversaries. Consequently, it is necessary, from a counter–directed energy weapons standpoint, to understand the effects of HEL on targets constructed with composite materials. Composites have become staples in both civilian and military sectors due to their desirable mechanical properties. They are stiff and lightweight, making them highly desirable for aircraft structures and thus have come into wide use in UAVs.[3,4] This was the motivation behind the current project as well as the desire to study HEL effects on carbon fiber composites. Although lasers are unlikely to leave gaping holes in targets such as UAVs, they can still inflict lethal damage due to internal thermal radiation. This problem has been investigated by scientists at the Materials Chemistry Branch of the Naval Research Lab. They noted that even without penetration, carbon fiber composites can reach temperatures up to 3000 °C, resulting in significant re-radiation to internal systems such as fuel tanks, batteries, and electronics. Because these systems may be only a short distance away from the skin, they are vulnerable to such damaging radiation.[5] UAVs can thus be damaged or destroyed when

internal components, such as lithium-ion batteries, become unstable around 150 °C, solder melts around 180 °C, and circuit boards char at approximately 300 °C.[6]

2. Experimental Approach

The objectives of this work were to reproduce and expand on the modeling conducted at the Navy Research Laboratory (NRL) and to validate the model experimentally. Following is a list of activities carried out in order to accomplish the project's objectives:

- Prepare thin carbon fiber composite materials, to include of 2-, 4-, and 6-ply sheets for testing.
- Predict the transient and steady-state back face temperatures of an irradiated composite with one-dimensional finite difference modeling.
- Use a high-temperature thermal imaging camera to record temperatures on the backside of an irradiated composite, and employ such temperatures to predict the temperature rise of a backside component.
- Use thermocouples to measure the temperature rise of a backside component at short distances.
- Validate the mathematical model by comparing the results against directly measured component temperatures and use these results to update and improve the model.

2.1. Preparation of carbon fiber–reinforced polymer (CFRP) composites

Each 12-inch by 12-inch composite laminate had a 50% carbon fiber–resin mass ratio, with the resin being prepared using a 100 to 26 weight ratio of DOW D.E.N 425 Epoxy Novalac and Dow Epikure W curing agent. The composites were reinforced with a 3K plain-weave, 5.7 oz/yd^2 carbon fiber cloth purchased from Fiber Glast Developments Corporation. The composites were first vacuum bagged for 1 h at 1 atm pressure in order to prevent air gaps and bubbles from forming between the plies. After the vacuum treatment, the composites were heated at 121 °C and cured using a 2-ton press for 1.5 hours. Prior to testing, the composite laminates were cut into 2-inch-wide (5.08 cm) strips, as shown in Fig. 1.

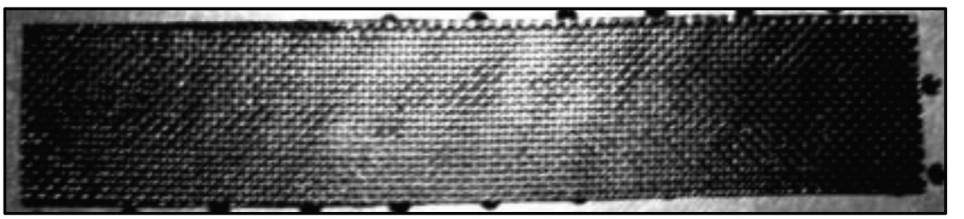

Fig. 1. 2-inch (5.08 cm) × 10-inch (25.4 cm) wide strip of carbon fiber composite prior to testing.

2.2. Laser power and irradiance

The laser used for this project was a YLR-100-AC IPG Photonics fiber laser. The IPG laser outputs a beam with an M^2 value of 1.07, indicating that the beam profile is close to Gaussian.

The laser has a maximum output of 100 W and, due to the laboratory setup, the minimum allowed output power was set at 20 W. Based on a 5-mm diameter beam, these limitations on the power meant that the range of on-target irradiances was between 101.9 W/cm^2 and 509.3 W/cm^2. This range was ideal for comparison to work done at NRL due to their significant research and study involving thin carbon fiber composites subject to irradiances between 50 W/cm^2 and 1000 W/cm^2.[5,6]

2.3. IR camera

A FLIR® A325sc infrared (IR) camera was used to measure the temperatures on the back of the irradiated CFRP. With the high temperature option and the FLIR ResearchIR Software, this camera is capable of measuring temperatures up to 2000 °C. Before temperature measurements were taken, the IR camera had to be calibrated to account for the emissivity of what is being viewed. Fig. 2 shows a preliminary test conducted to determine the emissivity of the carbon fiber fabric.

Four plies of carbon fiber were placed on a hot plate and had a Type K thermocouple woven between the fiber tows. The temperature of the carbon fiber was elevated to approximately 400 °C, with both the IR camera and thermocouple simultaneously recording temperatures. The emissivity input for the IR camera was adjusted until the camera displayed the same temperature as the thermocouple. The carbon fiber emissivity was determined to be 0.90, which is close to the literature value of 0.91 used by Tresansky.[7]

2.4. Internal component

Components behind the irradiated carbon fiber composite were simulated using a 1-cm diameter metal disc, made from 1008 carbon steel with a nominal thickness of 0.15 mm. Because of the steel's thinness, its front temperature was approximated as being equal to its back temperature. This temperature was measured with an attached Type K thermocouple. The disc was painted black with Champion heat-resistant spray paint so that 0.95 absorptivity could be assumed.[8] Fig. 3 shows a side view of the experimental setup. Note that the glass pipette in the center of the figure was used to hold the thermocouple and steel disc at the appropriate location behind the composite and that the steel disc was attached to the thermocouple using 450-20R solder, a high-temperature lead-free solder. It was assumed that the added mass from the solder did not significantly affect the heat capacity and transient temperature rise of the steel disc.

2.5. Experimental setup

Figure 4 shows a top-down view of the experimental setup. The IR camera was offset 53 degrees from perpendicular to avoid the possibility of damage in case the laser penetrated the composite. The red dashed line represents the laser beam and the blue dashed lines the camera field of view.

Figure 5 shows a rear view of the experimental setup. The vacuum was used to remove smoke from the test area and the thermopile was used to absorb laser irradiation in case of target penetration. As a safety precaution, nitrogen gas was used to extinguish fires that were large enough to potentially cause damage to surrounding equipment and personnel.

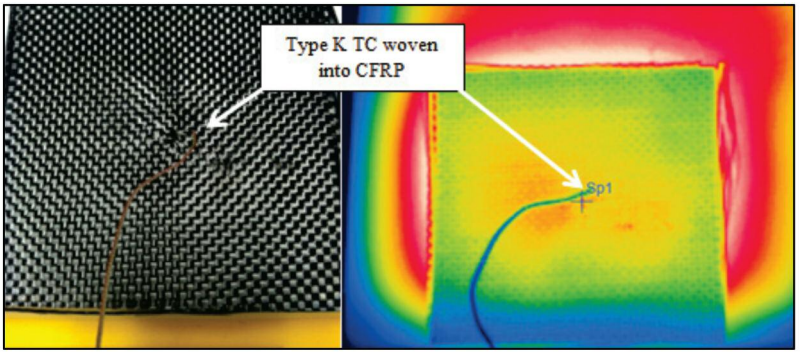

Fig. 2. Visual and IR images of heated carbon fiber composite.

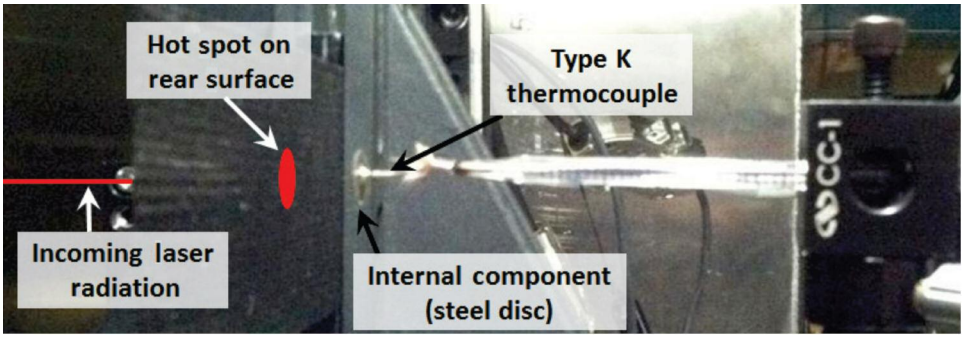

Fig. 3. Side view of composite strip and back side component.

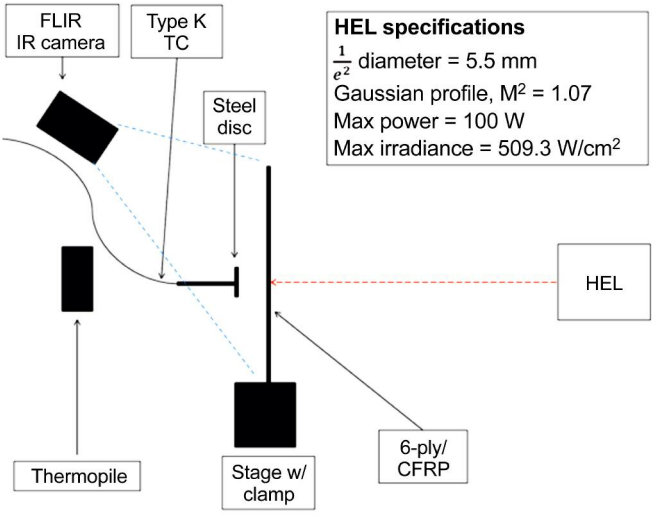

Fig. 4. Top-down view of experimental setup.

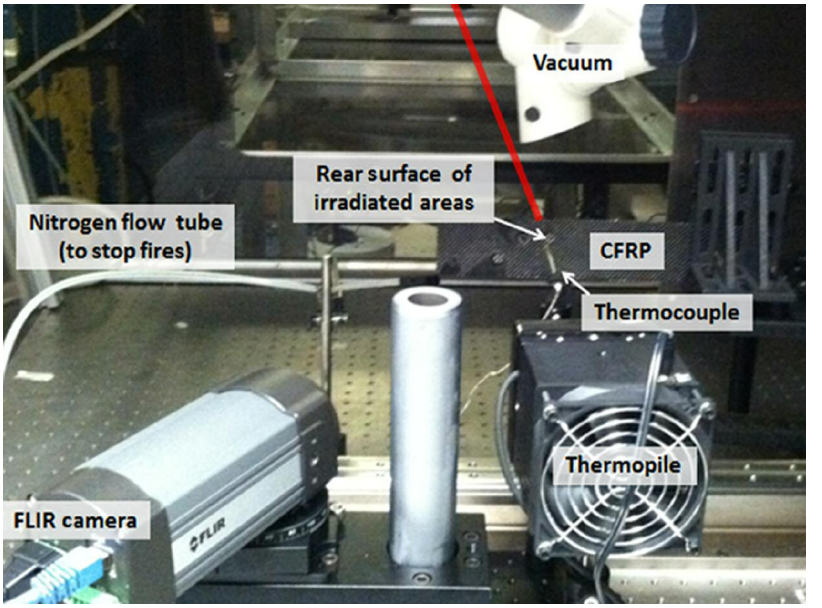

Fig. 5. Rear view of experimental setup.

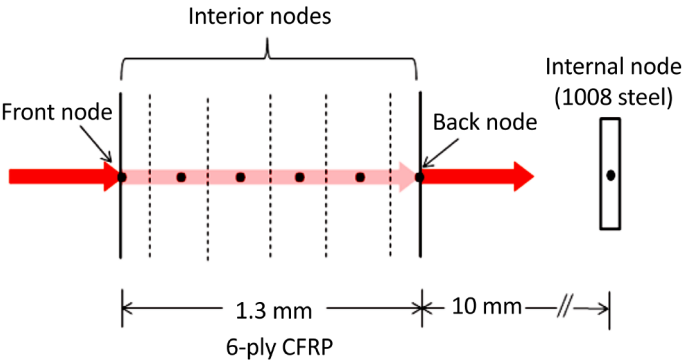

Fig. 6. 1D finite difference approach. (Note: Image not to scale.)

3. Modeling Approach

An explicit unidimensional finite-difference heat transfer approach was used to model re-radiation from a carbon fiber composite to internal components. This involved discretizing the 1D heat equation, Eq. (1), with no energy generation in terms of space and time to obtain a numerical solution.

$$\frac{\partial}{\partial x}\left(k\frac{\partial T}{\partial x}\right)=\rho c_p\frac{\partial T}{\partial t} \tag{1}$$

Figure 6 shows a visual representation of this approach.

Equation (2) was used to calculate the temperatures of the front node, Eq. (3) was used to calculate interior node temperatures, and Eq. (4) was used for the back node. Each of these equations calculated the temperature at the next time step, T^{p+1}, based on the temperature at the previous time step, T^{p}. The subscript identifies node location, with T_1 being the temperature of the front node, T_m representing the middle nodes, and T_n representing the temperature of the back node/surface. Eq. (2) accounts for the heat flux (heat transferred per unit area), conduction through the surface, convective cooling of the surface, and radiative heat transfer from the surface.

$$T_1^{p+1} = \frac{2\Delta t}{\rho c_p \Delta x}\left(q'' + k\ \frac{(T_2^p - T_1^p)}{\Delta x} + h\left(T_\infty - T_1^p\right) + \epsilon\sigma\left(T_\infty^4 - T_1^4\right)\right) + T_1^p \tag{2}$$

Because the interior nodes were not subject to laser irradiation, convection, or radiation, Eq. (3) only accounted for conduction into and out of each node.

$$T_m^{p+1} = \frac{\Delta t * k}{\rho c_p \Delta x^2}(T_{m+1}^p + T_{(m-1)}^p - 2T_m^p) + T_m^p \tag{3}$$

Similar to Eq. (2), Eq. (4) accounted for conduction to the back surface, convective heat transfer, and radiative heat transfer. This equation did not include a heat flux term because the back surface was not subject to incident laser irradiation.

$$T_n^{p+1} = \frac{2\Delta t}{\rho c_p \Delta x}\left(k\frac{(T_{n-1}^p - T_n^p)}{\Delta x} + h\left(T_\infty - T_n^p\right) + \epsilon\sigma\left(T_\infty^4 - T_n^4\right)\right) + T_n^p \tag{4}$$

Table 1 shows the parameters used to perform the calculations in MATLAB®. It was assumed that the initial temperature of the composite and the temperature of the surroundings were equal to the air temperature of 293 K.

Table 1. Material properties and model parameters

Parameter	Units	Variable	Value
Initial temperature	K	T_i	293[a]
Air temperature/surrounding temperature	K	T_∞	293[a]
Convection coefficient	W/m^{2}K	h	25[a]
Beam radius	m	r	0.0025[a]
Carbon/epoxy composite through thickness thermal conductivity	W/mK	k	0.61[b]
Carbon/epoxy composite density	kg/m^3	p	1700[b]
Carbon/epoxy composite specific heat	J/kgK	c_p	1500[b]
Carbon/epoxy composite emissivity	NA	ε	0.91[b]
Time step	sec	Δt	0.001
Distance between nodes	m	Δx	0.00025
Carbon/epoxy composite thickness	m	L	0.0013[a]
1008 steel density	kg/m^3	p_s	7872[b]
1008 steel specific heat	J/kgK	c_{ps}	481[b]
Painted 1008 steel emissivity	NA	ε_s	0.95[b]

[a] Properties measured/calculated at USNA.[6]

[b] Properties from the literature.

4. Results and Discussion

4.1. Experimentation

Figure 7 shows the time–temperature response of five different tests in which a 6-ply carbon fiber composite was irradiated for 60 s. The irradiances varied between 152.8 W/cm^2 and 356.5 W/cm^2, and the temperatures measured were at the center of the hotspot. The hotspot was defined as the area on the back of the composite affected by the laser. It is important to note that while the composite was at room temperature (293 K) at the beginning of testing, the IR camera indicated that the initial temperature was closer to 400 K. This difference was due to the camera being adjusted to its high temperature option and only being able to accurately measure temperatures between 573 K and 2273 K.

The increase in temperature at the end of the 356.5 W/cm^2 test was likely due to laser induced recession through the thickness of the carbon fiber composite. Visual inspection of the area after testing confirmed that the laser had partially penetrated through the thickness of the composite, likely decreasing the resistance to heat transfer and increasing the temperature of the back surface. The rapid increase in the measured temperature may have also been due to a change in the emissivity of the carbon fiber composite as the epoxy was burned off. Due to rapid heating of the material, it is likely that its emissivity varied during the tests, thereby altering the recorded temperatures of the FLIR camera. Figs. 8 and 9 show the front and back surfaces of the tested composite.

The charring seen in Fig. 9 can be attributed to flames on the front side, as seen in Fig. 8. During these tests, there were no flames present on the back surface.

The next set of tests was conducted under the same conditions, but with a 1-cm diameter steel disc placed 1 cm behind the composite. Interestingly, each test resulted in significantly

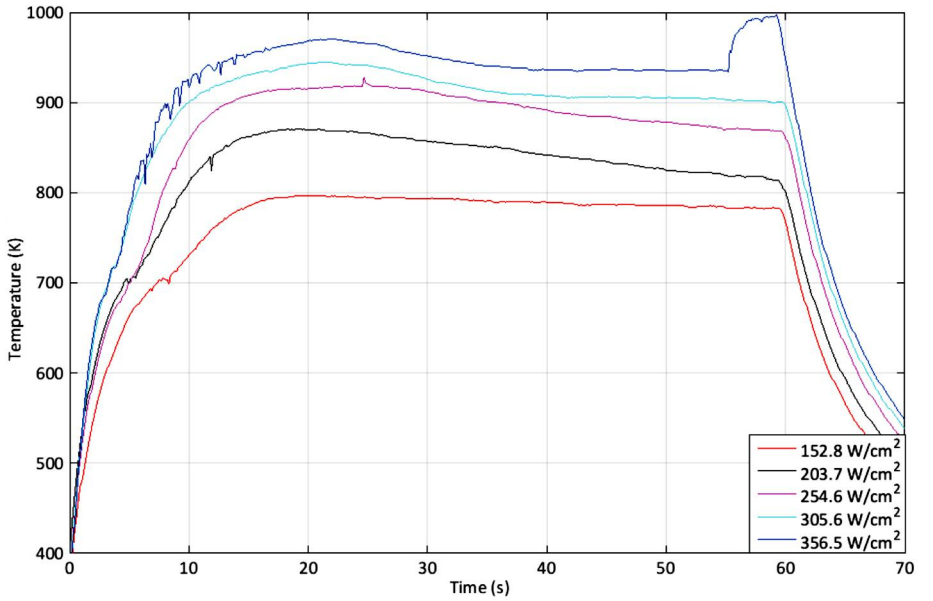

Fig. 7. 6-ply carbon fiber composite back surface irradiated for 60 s at varying irradiances.

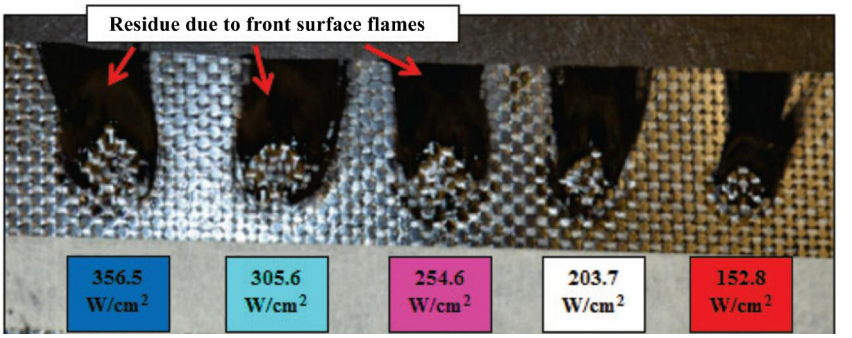

Fig. 8. Front surface of 6-ply CFRP.

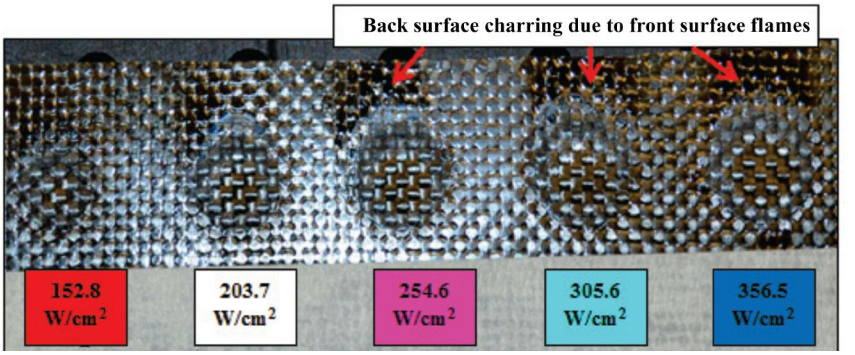

Fig. 9. Back surface of 6-ply CFRP.

higher temperatures accompanied by flames on the back surface of the composite. As the addition of the steel disc was the only change in the experiment, it was likely reflecting and also radiating heat back to the back surface. This additional heat is what raised the temperature of the resin high enough to initiate flames on the back surface. Fig. 10 compares the IR camera measurements of the 305.6 W/cm^2 test without a steel disc to the 305.6 W/cm^2 test with the steel disc. The excess heating due to the presence of the steel disc is clearly visible and corresponds to the back face flames recorded by the IR camera between approximately 12 s and 25 s. Once the fuel (resin) was burned off, the temperature of the composite cooled and approached the temperature it had been before the combustion event (~900 K). This temperature was close to the steady-state temperature of the composite tested without a steel disc. This was expected as the test without a steel disc did not involve flames on the back surface. Also shown in Fig. 10 is the temperature of the steel disc, which increased 188 K in 30 s. The peak increase in temperature of the steel disc occurred a few seconds after the back surface of the composite reached its peak temperature.

Figure 11 shows the front and back surfaces for both of the 305.6 W/cm^2 tests. The two images in the left side of Fig. 11 are the front and back surfaces without a steel disc (taken from Figs. 8 and 9) and the two images in the right side of Fig. 11 are the front and back surfaces at the same irradiance, but with the internal component being present during the

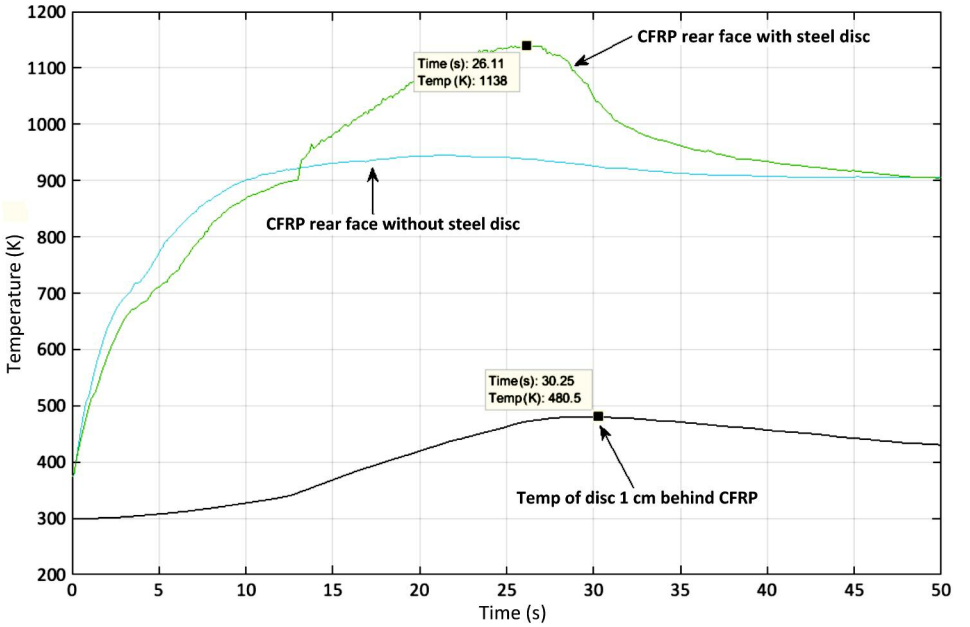

Fig. 10. 305.6 W/cm^2 without steel disc vs. 305.6 W/cm^2 with steel disc.

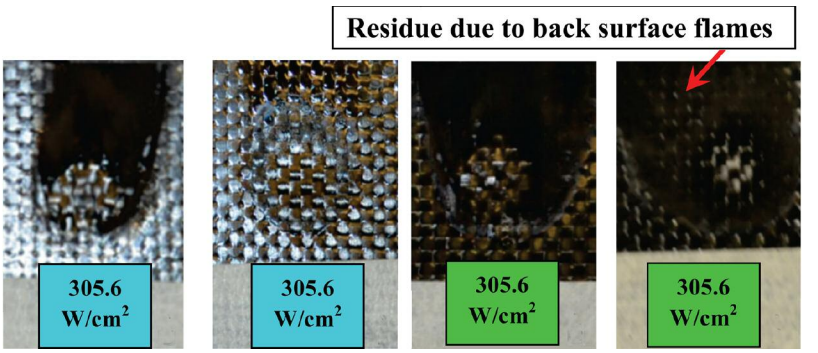

Fig. 11. 6-ply CFRP irradiated at 305.6 W/cm^2 with and without internal component. The two images on the left are from the test without the steel disc and the two images on the right are from the test with the steel disc.

test. The images show the residue/soot left by the back surface flames in the tests that incorporated the steel disc.

Next, Fig. 12 compares the IR camera measurements of the 356.5 W/cm^2 test without a steel disc to the 356.5 W/cm^2 test with the steel disc. As seen in the other tests that incorporated the steel disc, the flames on the back surface resulted in a significant temperature rise. During this test, the composite reached 1189 K after 24.5 s of laser irradiation. This was 223 K greater than the temperature of the composite 24.5 s into the test without the steel disc. Figure 12 also shows a rapid drop in temperature of the steel disc after it reached a peak of 502.4 K. This was because the steel disc was hot enough that the solder connecting

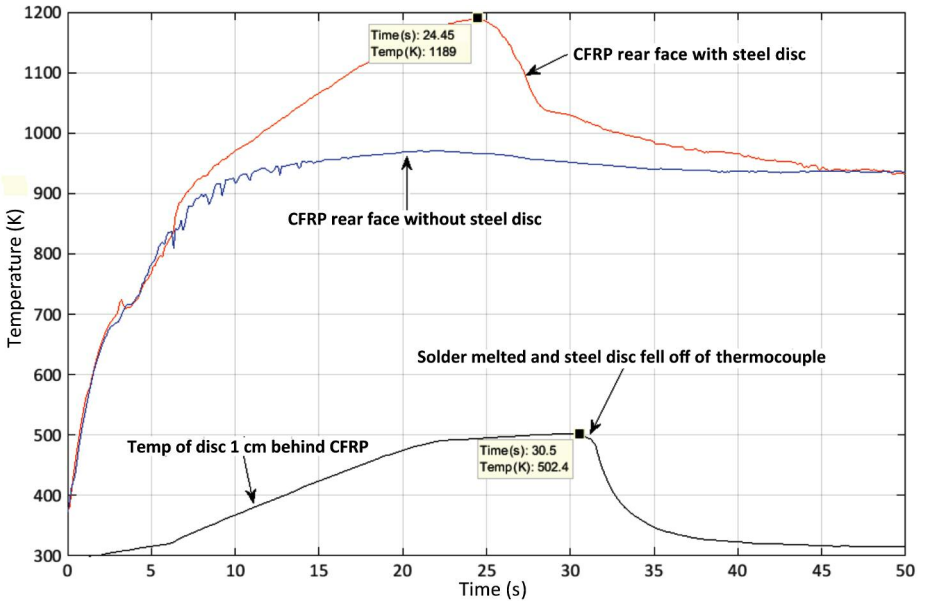

Fig. 12. 356.5 W/cm^2 without steel disc vs. 356.5 W/cm^2 with steel disc.

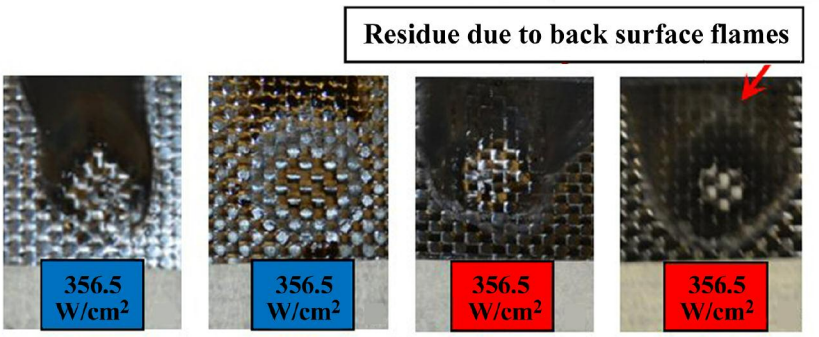

Fig. 13. 6-ply carbon fiber composite irradiated at 356.5 W/cm^2 with and without internal component. Two images at left are from test without steel disc and two images at right are from test with steel disc.

it to the thermocouple melted, causing the steel disc–thermocouple connection to fail. This failure of the internal component illustrates the danger high-energy lasers pose to UAVs whose electronic systems and circuits likely use materials similar to the solder used in this experiment. This also served to validate the thermocouple measurements because the melting point for this type of solder is between 505 K and 511 K.[9]

Similar to what is shown in Fig. 11, Fig. 13 confirms that the presence of the steel disc resulted in back surface flames. The two images on the left are from the test without the steel disc and the two images on the right are from the test with the steel disc.

The results shown in Fig. 13 indicate that the presence of the steel disc contributed to heating the composite. During the initial tests, the hotspot on the surface of the composite

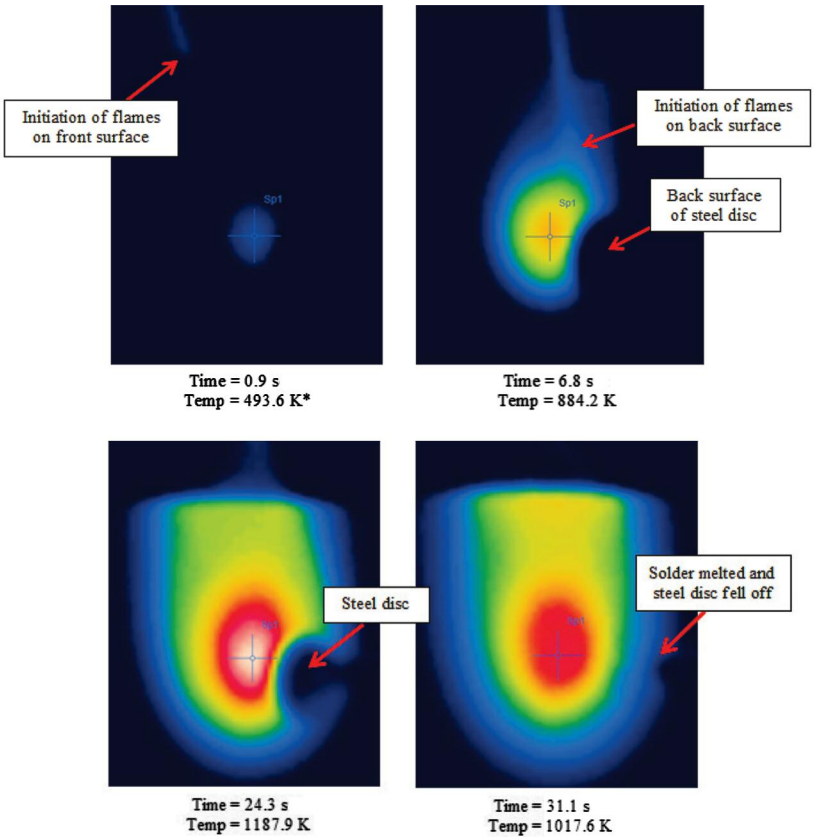

Fig. 14. IR images, back surface of 6-ply carbon fiber composite irradiated for 60 s at 356.5 W/cm^2 with steel disc 1 cm behind. (Note: This value is not accurate because camera range of measurement was 573 K to 2273 K.)

radiated heat to the surroundings. However, when the steel disc was in close proximity to the hotspot, some of the heat that had previously been radiated into the surroundings was instead absorbed by the steel disc and radiated back to the composite. Additionally, the steel disc likely reflected some of the radiation back to the composite, raising the temperature of the carbon fiber composite enough to initiate back side flaming. Fig. 14 shows IR images during the 356.5 W/cm^2 test and indicates when the steel disc fell off the thermocouple.

4.2 Modeling results

Figure 15 shows a comparison of the experimental and model results for 305.6 W/cm^2. As shown in the figure, the 1D finite difference model did not agree with the experimental results. This model assumed that heat flowed in one direction through the composite and parallel to the incoming radiation, but it did not account for heat flowing along the fibers and perpendicular to the incoming radiation. Furthermore, this model did not take into account changing material properties of the carbon fiber composite. When subject to intense heating,

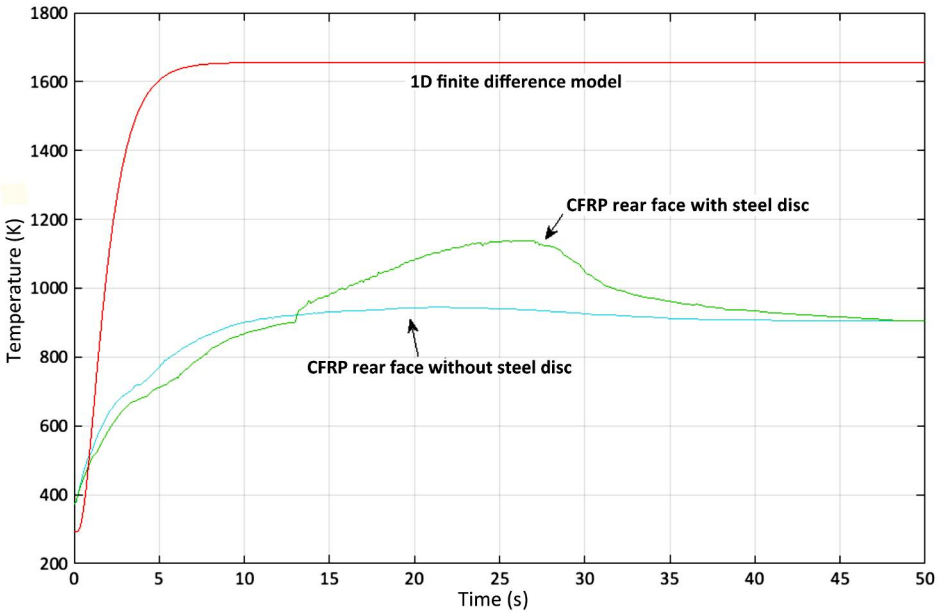

Fig. 15. 1D model vs. experimental results for back surface of 6-ply carbon fiber composite (CFRP) irradiated at 305.6 W/cm^2.

material properties such as specific heat, translucence, and thermal conductivity can change significantly. In addition, during heating the resin is burned out of the composite and the fibers begin to oxidize, certainly changing the material properties. Finally, during the tests the thickness of the composite in the irradiated area was changing as fibers were oxidized, ejected, and occasionally fell out due to structural instability. Although the model did not agree with the back face temperatures measured at U.S. Naval Academy (USNA), it was possible that the back face IR temperature measurements were not accurate. To investigate this, further tests were conducted during which IR camera measurements were compared to temperatures measured by fiber Bragg grating (FBG) sensors embedded in a thin carbon-fiber composite.

4.3. IR camera temperature measurement validation

In order to validate the IR camera measurements, FBG sensors were embedded in a 2-ply composite, which was then irradiated with the HEL at approximately 50 W and a 5-mm diameter spot size, for an effective irradiance of approximately 250 W/cm^2. The data from the FBG sensors in the rear ply were compared to data from the IR camera, which was pointed at the back of the CFRP. FBGs or fiber Bragg sensors can be used in conjunction with an interrogator to measure changes in temperature. The interrogator passes light through the optical fiber and some of it is reflected back by the grating. The peak wavelength of the reflected light, the Bragg wavelength, shifts due to changes in fiber temperature and strain. Because this relationship is well characterized, changes in the peak wavelength measured by the interrogator can be used to determine the change in temperature of the composite.[10]

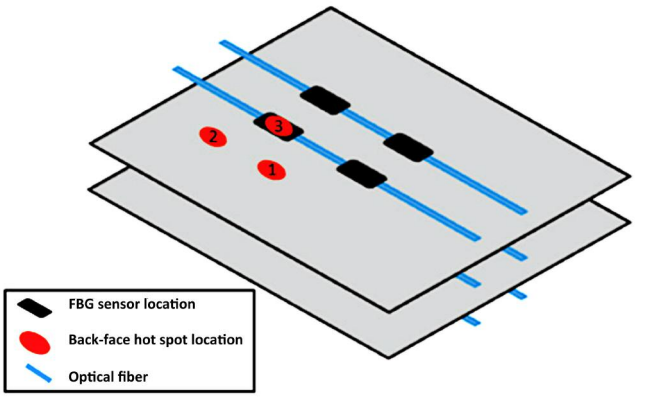

Fig. 16. Rear-view schematic of composite with embedded FBG sensors.

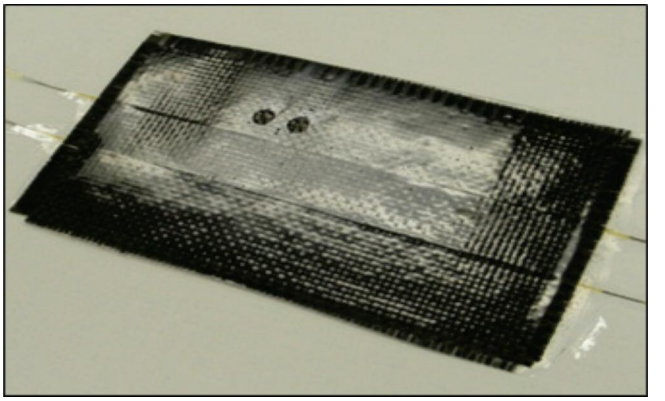

Fig. 17. 2-ply CFRP with embedded FBG sensors.

During the first test, the composite was irradiated approximately 1 cm below and 1 cm to the left of the FBG, and during the second test the composite was irradiated 1 cm below and 1 cm to the right of the FBG. For the third test, the FBG sensor was subject to direct laser irradiation. During each of these tests, a flow of nitrogen was used during the entire laser strike (5–25 s) to protect the FBG sensors by extinguishing ensuing flames. Fig. 16 shows a back-face view of the construction of the 2-ply composite with embedded FBG sensors, and Fig. 17 shows the actual CFRP sample before testing. The composite had multiple sensors embedded in the front, middle, and back layers; it was generally observed that the temperature shift measured by sensors was approximately the same in the different layers; this makes sense since the composite is very thin. Only the FBG sensor closest to the laser strike on the back face was used for comparison to the FLIR video of the back face.

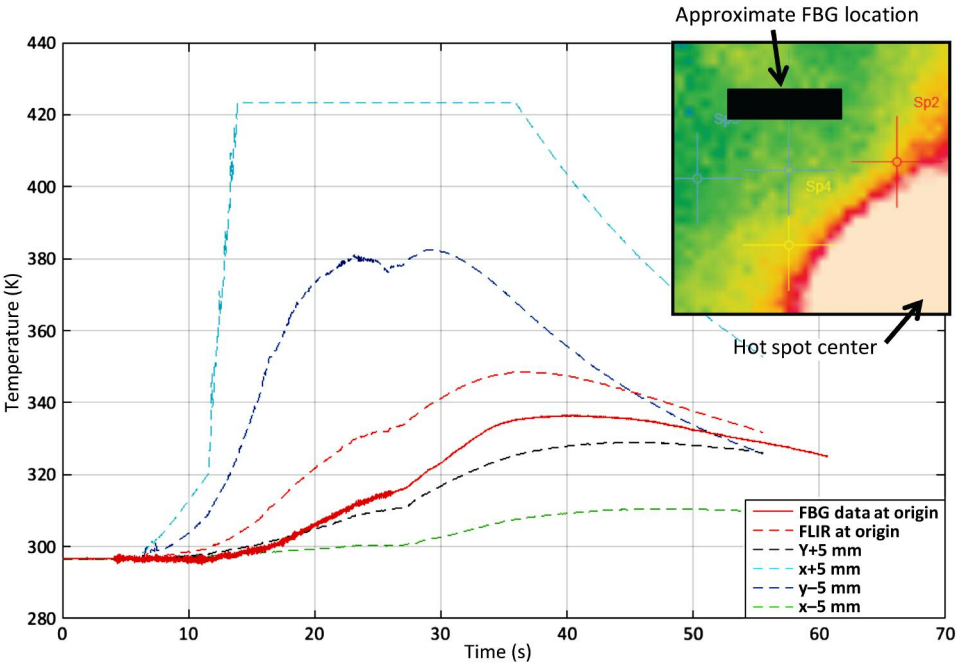

Fig. 18. First FBG comparison to IR data.

Figure 18 shows the results from the first FBG test during which the laser was aimed below and to the left of the sensor. An IR image of the back face is shown on the right side of this figure. During these tests, a CFRP emissivity value of 0.95 was used. The IR camera was set on the low temperature calibration range for this first test. The cursors shown on the right side of Fig. 18 measured the temperature in five locations that were near the estimated position for the FBG. The center cursor was called the "FLIR at origin" curve, with the other measurements being taken within 5 mm of that spot. Multiple measurements of the area of interest were taken because there was some uncertainty about the exact location of the FBG sensor. During this test, the IR camera was set to its low temperature range and did not record temperatures above approximately 420 K. This explains the plateau shape of the "x + 5 mm" curve shown in Fig. 18. The large spatial temperature gradient on the CFRP accentuates the importance of alignment between the FBG sensor and the image interrogation window. Fortunately, time histories of the temperature data can be used as a secondary indicator of position. Due to the transient nature of the laser strike, different positions on the CFRP reach peak temperature at different times. By looking at correlations of the time–temperature data at various interrogation windows, the proper location of the FBG within the IR camera image was confirmed. Fig. 18 shows that the FBG measurements from the back layer served to validate the IR temperature data, as the "y + 5 mm" temperatures were close to the "FBG data at origin" temperatures. Changes in the location of the cursor had a much more significant effect on the measured temperature than the assumed emissivity value.

Two other observations vis-à-vis Fig. 18 are noteworthy. The "noise" in the FBG data is due to vibrational strains induced in the composite by the N_2 gas used to suppress

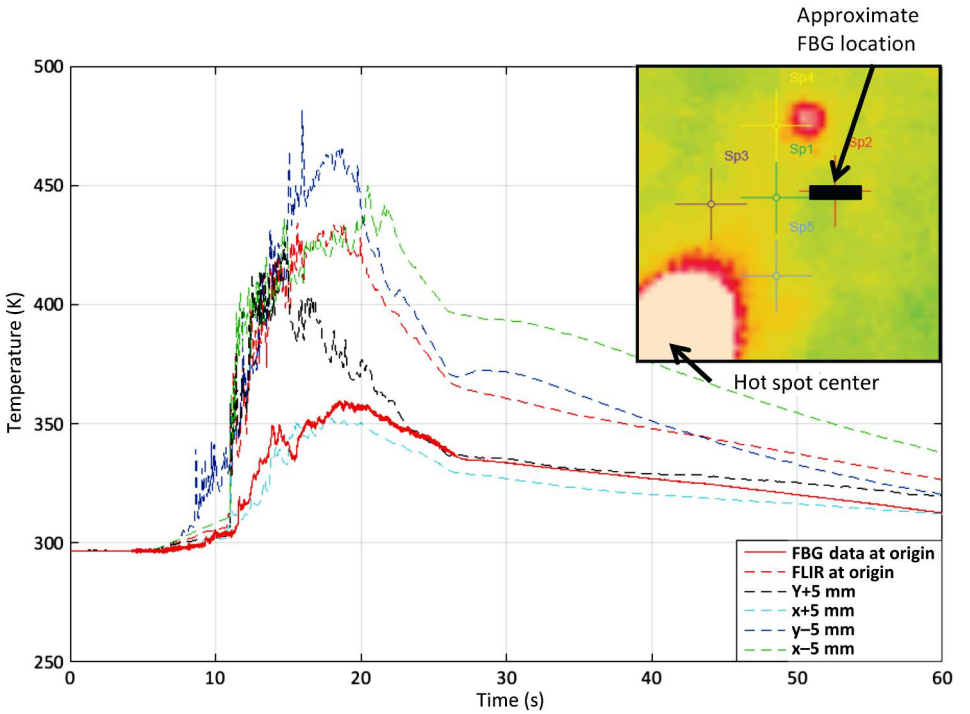

Fig. 19. Second FBG comparison to IR data.

combustion. The noise is eliminated at 25 s when the N_2 gas is turned off and the vibrations stop. But the temperature of the composite continues to rise, especially for locations in the IR image farthest from the hotspot, which is due to the relatively low thermal conductivity of the CFRP. The through-thickness FBG sensors exhibited similar temperature responses in the front and middle planes throughout the laser strike.

Figure 19 shows results from the second FBG test during which the laser was aimed below and to the right of the sensor. The laser power was reduced to 20 W (effective irradiance of 100 W/cm^2) and the IR camera was set on the mid-range temperature calibration for this second test; hence the more sensitive temperature results compared to the first test (Fig. 18). Temperatures recorded by the FBG in the second test (Fig. 19) are slightly higher than those of the first test (Fig. 18) because the flames were directed away from the FBG by the vacuum in the first test. As with the previous test, there was some uncertainty concerning the exact location of the FBG sensors relative to the laser spot. Fig. 19 shows that the "x + 5 mm" temperatures were in best agreement with the "FBG data at origin" temperatures recorded by the sensor in the back layer.

Next, Fig. 20 shows the results from the third FBG test. During this test, the laser was targeted directly at the FBG sensor. The laser power was 20 W and the IR camera was set on the high temperature range for this test. The relative size of the FBG sensor compared to the hotspot resulting from the laser strike meant that it was unnecessary to take multiple FLIR measurements of the region of interest. The FBG sensor on the back layer and IR data agreed from approximately 425 K to 1000 K. Above this temperature range, the FBG sensor

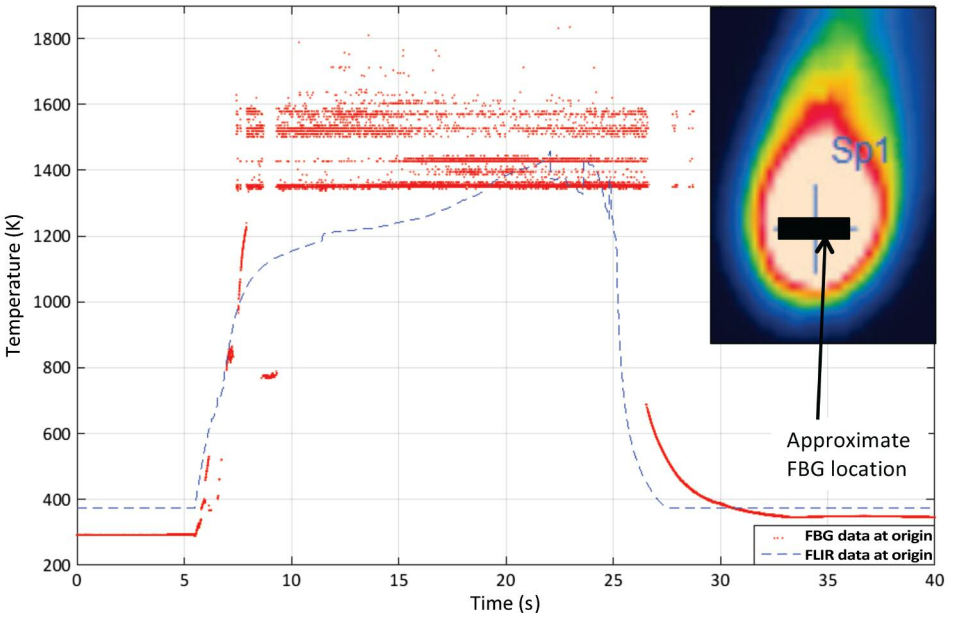

Fig. 20. Third FBG comparison to IR data.

began degrading[11] and the interrogator was unable to identify the Bragg or peak wavelength.[12] Even more rapid decay of the FBG sensors on the front and middle layers was observed within 6 s after the strike began. Interestingly, after the laser was shut off at 25 s and the CFRP and FBG lowered in temperature, the FBG "recovered" and the FBG data once again matched the IR camera data.

Conclusions and Future Work

The goal of this project was to investigate radiation from the back surface of a CFRP and its effects on an internal component. These experiments were intended to simulate the use of a directed energy weapon against a military vehicle comprised of a thin CFRP skin over an understructure, such as a UAV. The results confirmed that even without complete penetration, the intense local heating caused by laser radiation on a CFRP can cause internal components to fail. Additionally, radiation from the heated internal component contributed to development of flames on the back surface of the CFRP. The problem of internal flames is significant because the heat released during these events elevated the temperatures of the 6-ply CFRP back surface by 237 K during the 305.6 W/cm^2 test and by 240 K during the 356.5 W/cm^2. Furthermore, the failure of the steel disc–solder–thermocouple configuration illustrated the threat that directed energy weapons pose to vehicles even when the laser is unable to penetrate the surface. In an actual UAV fuselage, any internal flames could damage flight control mechanisms, ignite the fuel bladder or fuel tank, and quickly destroy the vehicle.

To successfully model this problem, more robust methods that are able to take into account the in-plane thermal conductivity of CFRPs and variable material properties are needed. Future work should investigate the effects of thermal barriers or coatings with

broadband reflective properties to reduce heat absorption of internal components. This could involve placing thin aluminum sheets between the steel disc and the CFRP, as aluminum is a broadband reflector, or painting the steel disc with a reflective paint with much lower absorptivity than the black paint used in this experiment. This would be an interesting problem to investigate, as the reflected radiation would heat the back surface of the CFRP, similar to how the heated steel discs radiated heat to the CFRP in the current experiment, and would likely result in additional flames and more damage to the CFRP.

Acknowledgments

This work was supported by the Office of Naval Research and the Joint Technology Office. The tests were conducted using the equipment and facilities provided by USNA's Directed Energy Research Center. We would like to thank Bob Cozzens, Matthew Evans, and Jesse Duncan of the Naval Research Laboratory for their significant guidance and input during this project. Brian Jenkins of the USNA Electrical and Computer Engineering Department was instrumental in helping with the fiber Bragg grating data acquisition, and data analysis. Also, Ralph Volino, Jim Cowart, and Patrick Caton of the USNA Mechanical Engineering Department provided great assistance and mentorship during the project.

References

1. Olson, M., History of Laser Weapon Research, in *Leading Edge*, **7**(4), Dahlgren, VA, Naval Surface Warfare Center, Dahlgren Division, Corporate Communication, 26–35.
2. All Systems Go: Navy's Laser Weapon Ready for Summer Deployment, April 7, 2014, accessed October 15, 2014 at http://www.navy.mil.
3. Low-Cost Composite Materials and Structures for Aircraft Applications, NATO/OTAN Science and Technology Organization Collaboration Support Office, accessed October 15, 2014, at http://ftp.rta.nato.int.
4. MQ-9 Reaper, U.S. Air Force, accessed October 14, 2014 at http://www.af.mil.
5. Cozzens, R., Evans, M., Duncan, J., High Energy Laser Lethality Involving Carbon Fiber Reinforced Composite Material. Naval Research Laboratory Memorandum Report NRL/MR/6120-1-9485, July 22, 2013.
6. Cozzens, R., Evans, M., Duncan, J., Response of Carbon Based Materials to High Energy Lasers, presented at DEPS CDEW Symposium, Albuquerque, NM, November 26–30, 2012.
7. Tresansky, A., Joyce, P., Radice, J., Watkins, J., J. Directed Energy, **5**, 159–174 (2014).
8. Radiation Surface Absorbers, Engineering Toolbox, accessed October 15, 2014, at http://www.engineeringtoolbox.com.
9. Solders, Fluxes, Kits, and Soldering Units, Micro-Measurements, A VPG Brand, accessed November 1, 2014, at http://www.vishaypg.com/docs/11023/soldacce.pdf.
10. Jenkins, B., Joyce, P., Mechtel, D., Milden, D., Elam, K., Watkins, J., Proc. SPIE **869308** (2013).
11. Erdogan, T., Mizrahi, V., Lemaire, P., Monroe, D., J. Appl. Phys. **76**(1), 73–80 (1994).
12. Webb, S., Peters, K., Zikry, M., Vella, T., Chadderdon, S., Selfridge, R., Schultz, S., Meas. Sci. Technol. **22**, 065301 (2011).